

A translatable RNAi-driven gene therapy silences *PMP22/Pmp22* genes and improves neuropathy in CMT1A mice

Marina Stavrou,¹ Alexia Kagiava,¹ Sarah G. Choudury,² Matthew J. Jennings,³ Lindsay M. Wallace,² Allison M. Fowler,² Amanda Heslegrave,^{4,5} Jan Richter,⁶ Christina Tryfonos,⁶ Christina Christodoulou,⁶ Henrik Zetterberg,^{4,5,7,8,9} Rita Horvath,³ Scott Q. Harper,^{2,10} and Kleopas A. Kleopa^{1,11}

¹Neuroscience Department, The Cyprus Institute of Neurology and Genetics, Nicosia, Cyprus. ²Center for Gene Therapy, The Abigail Wexner Research Institute at Nationwide Children's Hospital, Columbus, Ohio, USA. ³Department of Clinical Neurosciences, University of Cambridge, Cambridge, United Kingdom. ⁴Department of Neurodegenerative Disease, University College London (UCL) Institute of Neurology, London, United Kingdom. ⁵UK Dementia Research Institute at UCL, London, United Kingdom. ⁶Molecular Virology Laboratory, The Cyprus Institute of Neurology and Genetics, Nicosia, Cyprus. ⁷Department of Psychiatry and Neurochemistry, Institute of Neuroscience and Physiology, The Sahlgrenska Academy at the University of Gothenburg, Mölndal, Sweden. ⁸Clinical Neurochemistry Laboratory, Sahlgrenska University Hospital, Mölndal, Sweden. ⁹Hong Kong Center for Neurodegenerative Diseases, Hong Kong, China. ¹⁰Department of Pediatrics, The Ohio State University School of Medicine, Columbus, Ohio, USA. ¹¹Center for Neuromuscular Disorders, The Cyprus Institute of Neurology and Genetics, Nicosia, Cyprus.

Charcot-Marie-Tooth disease type 1A (CMT1A), the most common inherited demyelinating peripheral neuropathy, is caused by *PMP22* gene duplication. Overexpression of WT *PMP22* in Schwann cells destabilizes the myelin sheath, leading to demyelination and ultimately to secondary axonal loss and disability. No treatments currently exist that modify the disease course. The most direct route to CMT1A therapy will involve reducing *PMP22* to normal levels. To accomplish this, we developed a gene therapy strategy to reduce *PMP22* using artificial miRNAs targeting human *PMP22* and mouse *Pmp22* mRNAs. Our lead therapeutic miRNA, miR871, was packaged into an adeno-associated virus 9 (AAV9) vector and delivered by lumbar intrathecal injection into C61-het mice, a model of CMT1A. AAV9-miR871 efficiently transduced Schwann cells in C61-het peripheral nerves and reduced human and mouse *PMP22* mRNA and protein levels. Treatment at early and late stages of the disease significantly improved multiple functional outcome measures and nerve conduction velocities. Furthermore, myelin pathology in lumbar roots and femoral motor nerves was ameliorated. The treated mice also showed reductions in circulating biomarkers of CMT1A. Taken together, our data demonstrate that AAV9-miR871-driven silencing of *PMP22* rescues a CMT1A model and provides proof of principle for treating CMT1A using a translatable gene therapy approach.

Introduction

Charcot-Marie-Tooth (CMT) disease includes a genetically heterogeneous group of inherited peripheral neuropathies with a prevalence of up to 1 in 2500 persons (1, 2). The autosomal-dominant demyelinating CMT neuropathy type 1A (CMT1A [Mendelian inheritance in man (MIM) 118220]) is the most common

type, accounting for more than 50% of all CMT cases and resulting from an intrachromosomal duplication spanning 1.4 Mb on human chromosome 17p12 (3). The responsible disease gene (*PMP22*) encodes the peripheral myelin protein of 22 kDa (*PMP22*), which is located within this duplicated region (4–7). Patients with CMT1A develop distal muscle weakness and atrophy as well as sensory loss and have absent reflexes, with typical onset in adolescence. CMT1A is slowly progressive, with marked variability in disease severity (8, 9). Sensory responses are usually absent, whereas motor nerve conduction velocities (MNCVs) are slowed, ranging from 5 to 35 m/s in the forearm, but most average around 20 m/s, with uniform and symmetric findings in different nerves. Although NCVs do not change significantly over decades, motor amplitudes and the number of motor units decrease slowly, reflecting axonal loss and correlating with progressive clinical disability.

PMP22 is mainly expressed by myelinating Schwann cells (SCs) and localized in compact myelin (10) but is also present in non-neural cell types such as fibroblasts, endothelia, and epithelia (11). Mouse studies support the idea that *PMP22* is

Conflict of interest: The sequences and methods described here were included in a provisional patent application filed on December 1, 2020 (PCT/US21/61177). SQH, KAK, and MS are listed as inventors. HZ has served on scientific advisory boards and/or as a consultant for Abbvie, Alecort, Annexon, Artery Therapeutics, AZTherapies, Cognition Therapeutics (CogRx), Denali Therapeutics, Eisai Company, NervGen Pharma, Novo Nordisk, Pinteon Therapeutics, Red Abbey Labs, Passage Bio, Roche, Samumed, Siemens Healthineers, Triplet Therapeutics, and Wave; has given lectures at symposia sponsored by Collectricon, Fujirebio, Alzecure, Biogen, and Roche; and is a co-founder of Brain Biomarker Solutions in Gothenburg AB (BBS), which is a part of the GU Ventures Incubator Program.

Copyright: © 2022, Stavrou et al. This is an open access article published under the terms of the Creative Commons Attribution 4.0 International License.

Submitted: March 2, 2022; **Accepted:** May 12, 2022; **Published:** May 17, 2022.

Reference information: *J Clin Invest.* 2022;132(13):e159814.

<https://doi.org/10.1172/JCI159814>.

normally involved in early steps of myelin formation and in the maintenance of myelin and axons in the PNS (12–15). In humans, *PMP22* mRNA and *PMP22* protein overexpression in nerve biopsies from patients with CMT1A indicates that increased *PMP22* dosage is the most likely disease mechanism underlying CMT1A (16–19). This hypothesis is further supported by a recapitulation of numerous CMT1A-associated phenotypes in *PMP22*-overexpressing rodent models (20–30), including C61-het mice (22), which contain 4 copies of WT human *PMP22* on a normal mouse background. The exact mechanisms by which *PMP22* overexpression causes CMT1A remain unclear but may involve proteasome dysfunction related to excessive amounts of *PMP22* protein. Specifically, in normal myelinating and nonmyelinating SCs, approximately 20% of newly synthesized *PMP22* is glycosylated, while the remaining approximately 80% is targeted for proteasomal endoplasmic reticulum-associated degradation (ERAD) (31). Thus, in CMT1A, overexpressed *PMP22* is thought to accumulate in perinuclear aggresomes (32, 33) and impair overall proteasome activity (34), resulting in myelin sheath destabilization in SCs and ultimately nerve dysfunction.

Based on this model, the most direct approach to CMT1A therapy will likely involve reducing overexpressed *PMP22* to normal levels in SCs. Prior attempts to accomplish this using drug-based approaches were unsuccessful in human clinical trials (NCT00484510, NCT02600286, NCT05092841, NCT04762758, NCT03023540), and to date, CMT1A remains intractable. Nevertheless, progress continues in the field, with prospective adjunct therapies approaching clinical trials (35–37) and several preclinical strategies to silence *PMP22* reported (38–61). For example, CRISPR/Cas9 was used to directly target the *PMP22* gene by deleting its regulatory regions with encouraging results *in vitro* (62) and *in vivo* (63), and oligonucleotides have been tested to inhibit *PMP22* via promoter disruption or through mRNA degradation using RNAase H or RNAi-based mechanisms (using DNA gapmers or siRNAs, respectively) in different CMT1A rodent models (64–67). Among these various silencing approaches, RNAi has so far been used most often as a prospective mechanism to develop a CMT1A therapy (68).

RNAi is a conserved process of gene silencing triggered by endogenous miRNAs, which are encoded in the genomes of eukaryotic organisms. Mature forms of natural miRNAs are small (approximately 22 nucleotides long), noncoding RNA molecules that negatively regulate the expression of a vast fraction of the transcriptome at the posttranscriptional level (69, 70). Importantly, natural miRNAs can be modified in the form of siRNAs, shRNAs, or artificial miRNAs and retargeted to specifically base pair with disease genes, triggering target mRNA degradation through the RNA-induced silencing complex (RISC). siRNAs are chemically synthesized, produce transient effects, and require repeated, lifelong administration to achieve long-term gene silencing. In contrast, shRNAs or artificial miRNAs can be cloned as DNA expression cassettes, delivered to target cells within viral vectors, and transcribed *in vivo* to produce long-term target gene silencing after 1 administration. As mentioned, siRNAs have been used to trigger RNAi against *PMP22* in at least 3 published studies (65, 67), but RNAi treatment of CMT1A in *in vivo* and *in vitro* models was also

achieved using gene therapy vectors expressing natural miRNAs (mir-29a; ref. 71 or mir-318; ref. 72) or by an intraneurally injected AAV2/9 vector expressing rodent *Pmp22*-targeting artificial shRNAs (73). These shRNAs contained mismatches with the human *PMP22* sequence and were not tested in models expressing human *PMP22*, so it is unclear if these sequences, as well as the invasive and laborious intraneural injection method, can be translated to humans (73).

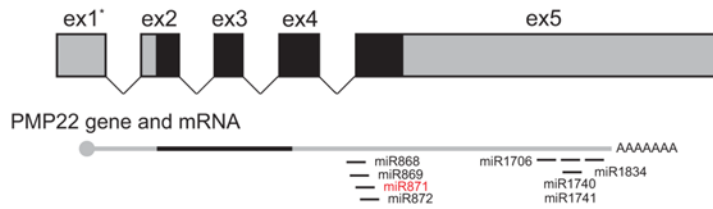
Here, we designed and tested a translatable AAV9-based gene therapy approach for CMT1A using an artificial miRNA targeting conserved regions on the human *PMP22* and mouse *Pmp22* transcripts. We demonstrate long-lasting therapeutic effects following a single, clinically relevant lumbar intrathecal injection in a mouse model of CMT1A that expressed both human *PMP22* and mouse *Pmp22* gene products. Thus, our study provides proof of principle for treating CMT1A with a gene therapy approach that uses artificial miRNA sequences and a route of administration that can be translated to human trials.

Results

Design and in vitro validation of artificial miRNAs to downregulate human and murine PMP22. Full-length human *PMP22* and mouse *Pmp22* are encoded by 5 exons, with 2 alternatively spliced first exons containing 5'-UTR sequences (ex1* 1a and ex1b). Both variants encode identical 483 bp ORFs and share the same 3'-UTR, which is located in exon 5 (ex5) (ORFs) (Figure 1A). To ensure that we targeted all *PMP22* transcripts, we excluded exon 1 from the query sequence and designed artificial miRNAs targeting human *PMP22* exons 2 to 5 (1655 nucleotides) using a previously described algorithm (74). This screen identified 117 candidates. Because we intended to use the RNA polymerase III-dependent (pol III-dependent) U6 promoter to drive miRNA expression, we excluded 29 of the 117 candidates because of the presence of RNA pol III termination sequences (5–6 T's) within the miRNA expression cassettes. The remaining 88 sequences were additionally filtered to ensure that the antisense guide strand of the miRPMP22 miRNAs would equally target human *PMP22* and mouse *Pmp22* sequences. Only 8 sequences (9%) showed this conservation, and all were located in exon 5, which encodes the 3'-UTR (Figure 1A and Supplemental Figure 1; supplemental material available online with this article; <https://doi.org/10.1172/JCI159814DS1>). Following cloning into a U6T6 expression plasmid, we empirically tested all 8 miRPMP22 miRNAs (miR868, miR869, miR871, miR872, miR1706, miR1740, miR1741, and miR1834) for silencing efficacy (Figure 1, B and C). Specifically, we cotransfected HEK293 cells with each individual U6-miRPMP22 plasmid and CMV-driven *PMP22* or *Pmp22* full-length cDNAs, and then harvested RNA 24 hours later, generated cDNA, and performed real-time quantitative PCR (RT-qPCR) using for *PMP22* or *Pmp22*, normalized to *RPL13A*. Negative controls included cells transfected with *PMP22* or *Pmp22* and U6.miRGFP (miRNA targeting EGFP) or an empty U6T6 plasmid (no miR). Data were collected and averaged from 3 independent experiments, with each RT-qPCR assay performed in triplicate. Although 7 of 8 miRPMP22s (87.5%) showed some level of silencing compared with the “no miR” control, only miR868 and miR871 showed

A miPMP22 design and selection criteria:

- 1) Mature guide strand with 22 nt base pairing with human *PMP22* mRNA (1,655 nt query, exons 2-5)
- 2) Selection based on percentage and distribution of GC content (117 candidates)
- 3) Absence of RNA pol III termination signal in miRNA sequence (88 of 117)
- 4) *PMP22* target site conservation in human and mouse (8 of 88)
- 5) *In vitro* gene silencing efficacy targeting mouse and human *PMP22* sequences



B miR-PMP22-871 (miR871)

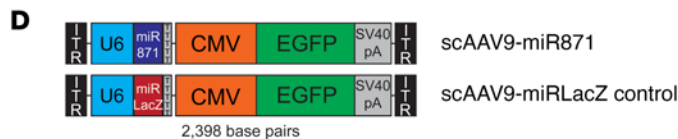
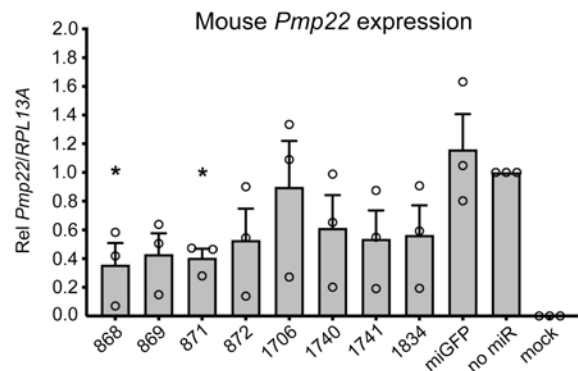
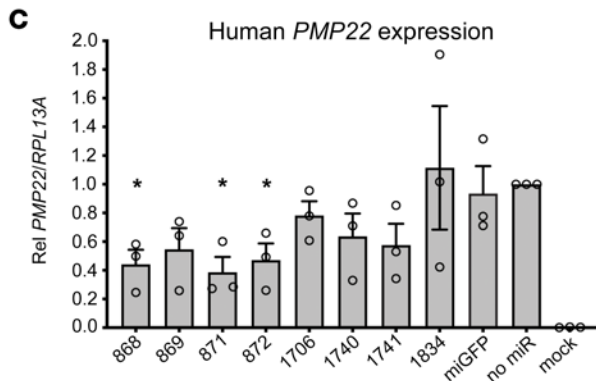
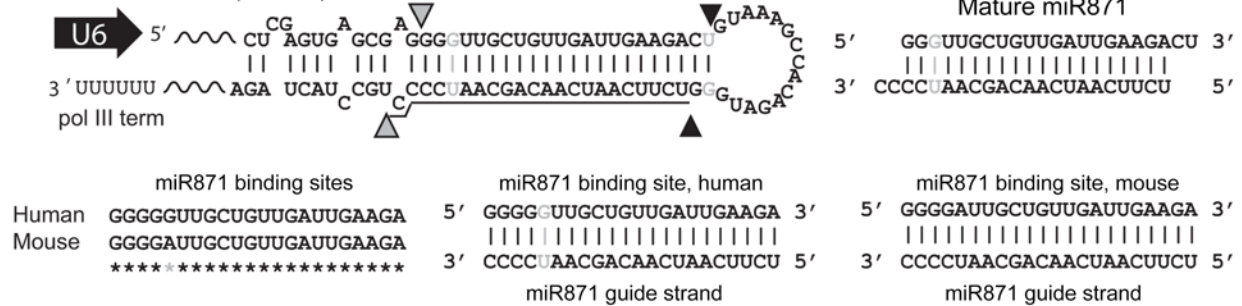


Figure 1. Design and in vitro screen of artificial miRNAs targeting PMP22. (A) Full-length *PMP22* mRNA was transcribed from 5 exons (ex), producing 2 major transcripts with identical ORFs (black shading). We designed 8 candidate miRNAs to equally target both human *PMP22* and murine *Pmp22* mRNAs. (B) Gray and black arrowheads show miR871 cut sites by Drosha and Dicer, respectively. dsRNAs form G:U wobble base pairs (indicated by gray shading). Underlined sequence represents the mature miR871 antisense guide strand. Bottom panel shows alignment of the miR871 binding site on human *PMP22* and murine *Pmp22* mRNAs. Gray asterisk indicates a G:A mismatch at the miR871 binding site, but each nucleotide at this location can form 2 hydrogen bonds with the miR871 guide strand as a G:U wobble (human) or A:U wobble (mouse). (C) RT-qPCR was performed to measure in vitro human *PMP22* or murine *Pmp22* silencing by the indicated miR871s ($n = 3$ /group). Gene expression was normalized to human *RPL13A*. * $P < 0.05$, by unpaired, 1-tailed Student's t test. Values represent the mean \pm SEM. Rel, relative. (D) Schematic of scAAV9, which was used to deliver miR871 or miRLacZ expression cassettes in vivo. The U6 promoter drives the transcription of miR871 or miRLacZ, and the CMV promoter drives the *EGFP* gene with the SV40 polyadenylation sequence.

statistically significant ($P < 0.05$) silencing of *PMP22* and *Pmp22* sequences. Because miR871 consistently silenced both genes by approximately 60%, we chose the miR871 sequence as our lead. The U6-miR871 sequence was then subcloned into a self-complementary adeno-associated virus (AAV) (scAAV. CMV.EGFP) backbone containing a separate CMV.EGFP

reporter gene (Figure 1D), and we generated AAV9 particles using triple transfection in HEK293 cells (hereafter referred to as AAV9-miR871). Lysates were purified by iodixanol-gradient ultracentrifugation and fast protein liquid chromatography (FPLC), as previously described (75). Similarly, we generated a control scAAV9.CMV.EGFP vector expressing a U6

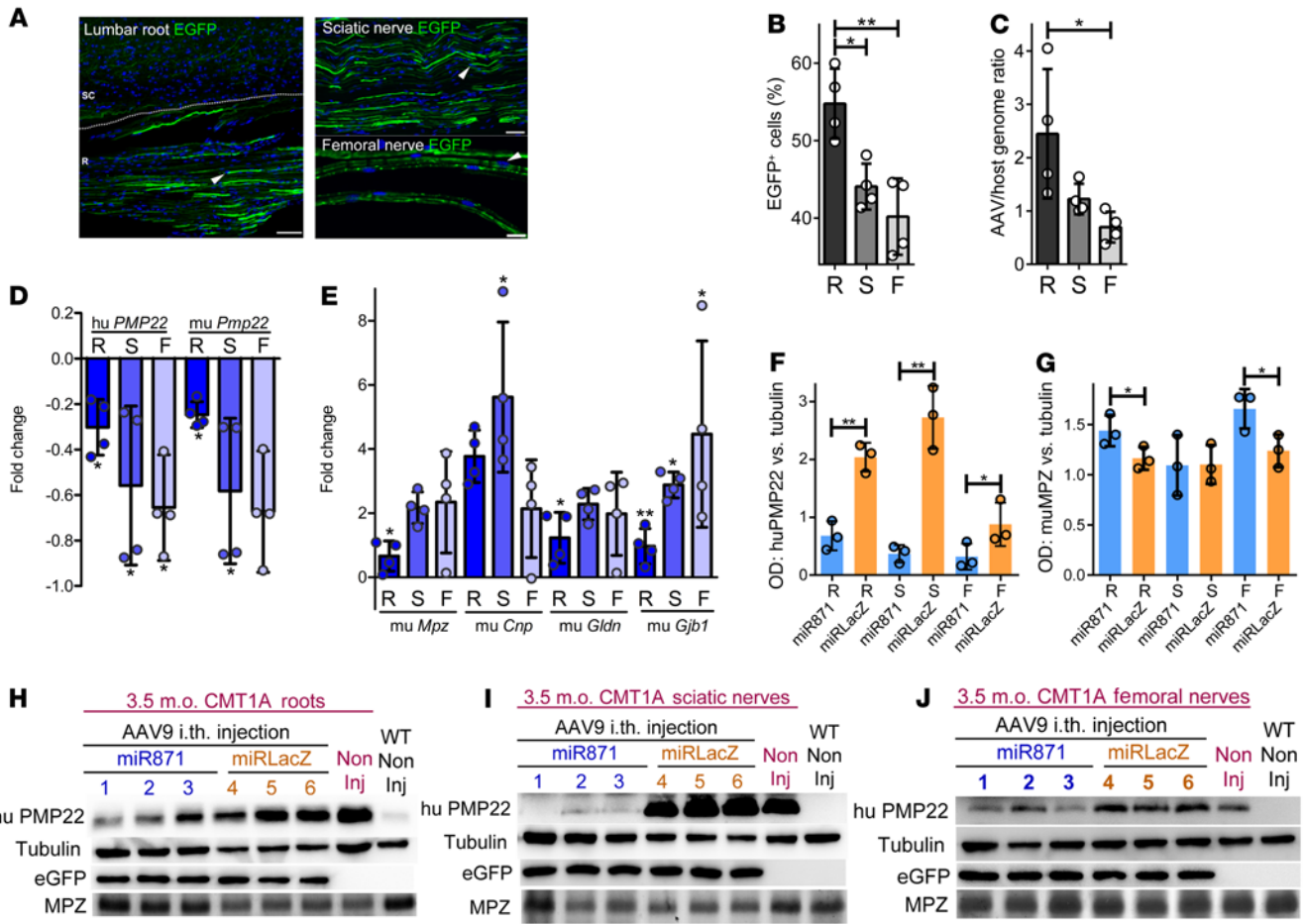


Figure 2. In vivo assessment of AAV9-miR transduction in PNS tissues and validation of AAV9-miR871 silencing efficiency in a CMT1A mouse model 6 weeks after injection. (A) Lumbar spinal roots and sciatic nerve sections as well as teased femoral nerve fibers showing EGFP autofluorescence in SCs and axons. Arrowheads indicate examples of EGFP⁺ nuclei. Scale bars: 60 μm (lumbar root and sciatic nerve) and 20 μm (femoral nerve). (B) Quantification of EGFP-expressing PNS cells (n = 4/group). (C) VGCNs (n = 4/group) confirmed peripheral nerve transduction. RT-qPCR analysis of (D) Human (hu) *PMP22* and murine (mu) *Pmp22* and of murine (E) *Mpz*, *Cnp*, *Gldn*, and *Gjb1* gene expression (n = 3/group). Fold changes in relative mRNA expression of CMT1A-AAV9-miR871 were calculated in comparison with expression levels in CMT1A-AAV9-miRLacZ mice. All samples were normalized to endogenous *Gapdh*. Quantification of (F) human PMP22 and (G) murine MPZ Western blot protein ODs, normalized to tubulin (Tub), in CMT1A-AAV9-miR871 and CMT1A-AAV9-miRLacZ mice in lumbar roots, sciatic nerves, and femoral nerves. Western blots showing human PMP22, murine tubulin, EGFP, and murine MPZ protein levels in (H) roots, (I) sciatic nerves, and (J) femoral nerves. Values represent the mean ± SD. *P < 0.05 and **P < 0.01, by 1-way ANOVA with Tukey’s multiple-comparison test. R, lumbar roots; S, sciatic nerves; F, femoral nerves; i.th., intrathecal; m.o., months old; Non Inj, noninjected.

promoter-driven miRNA targeting the *E. coli LacZ* gene (hereafter referred to as AAV9-miRLacZ).

Biodistribution and expression following lumbar intrathecal injection of AAV9-miR871. We delivered the AAV9-miR871 vector expressing the EGFP gene under the CMV promoter into 2-month-old C61 heterozygous mice (22) (hereafter referred to as the CMT1A mouse) using lumbar intrathecal injection (20 μL containing a total of 5e11vg/mouse). Six weeks after injection, we examined AAV9-miR871 biodistribution and transduction in PNS cells. For this purpose, we used vector genome copy numbers (VGCNs) and EGFP expression analysis in anterior lumbar roots and sciatic and femoral nerves. EGFP was detected as autofluorescence in the perinuclear cytoplasm of a subset of PNS cells as well as in the axons of lumbar roots and sciatic and femoral nerves (Figure 2A). The percentage of EGFP-expressing

SCs in immunostained tissue sections reached an average of 54.78% ± 4.53% in anterior lumbar roots, 44.07% ± 2.96% in sciatic nerves, and 40.18% ± 4.93% in femoral nerves (n = 4 mice; Figure 2B). VGCNs in DNA extracted from PNS tissues reached 2.44 in anterior lumbar roots, 1.23 in sciatic nerves, and 0.69 in femoral nerves (n = 4 mice; Figure 2C).

In vivo validation of AAV9-miR871-mediated silencing of the PMP22 gene in CMT1A mice. Prior to any treatment studies, we performed a detailed characterization of baseline functional and morphological deficits of the C61-het CMT1A mouse line, which contains 4 copies of the human *PMP22* gene and 2 normal copies of murine *Pmp22*, compared with WT mice at 2, 4, 6, 8, and 10 months of age. We confirmed progressive functional impairment associated with early-onset demyelination (Supplemental Figures 2-7). We also assessed the potential toxicity

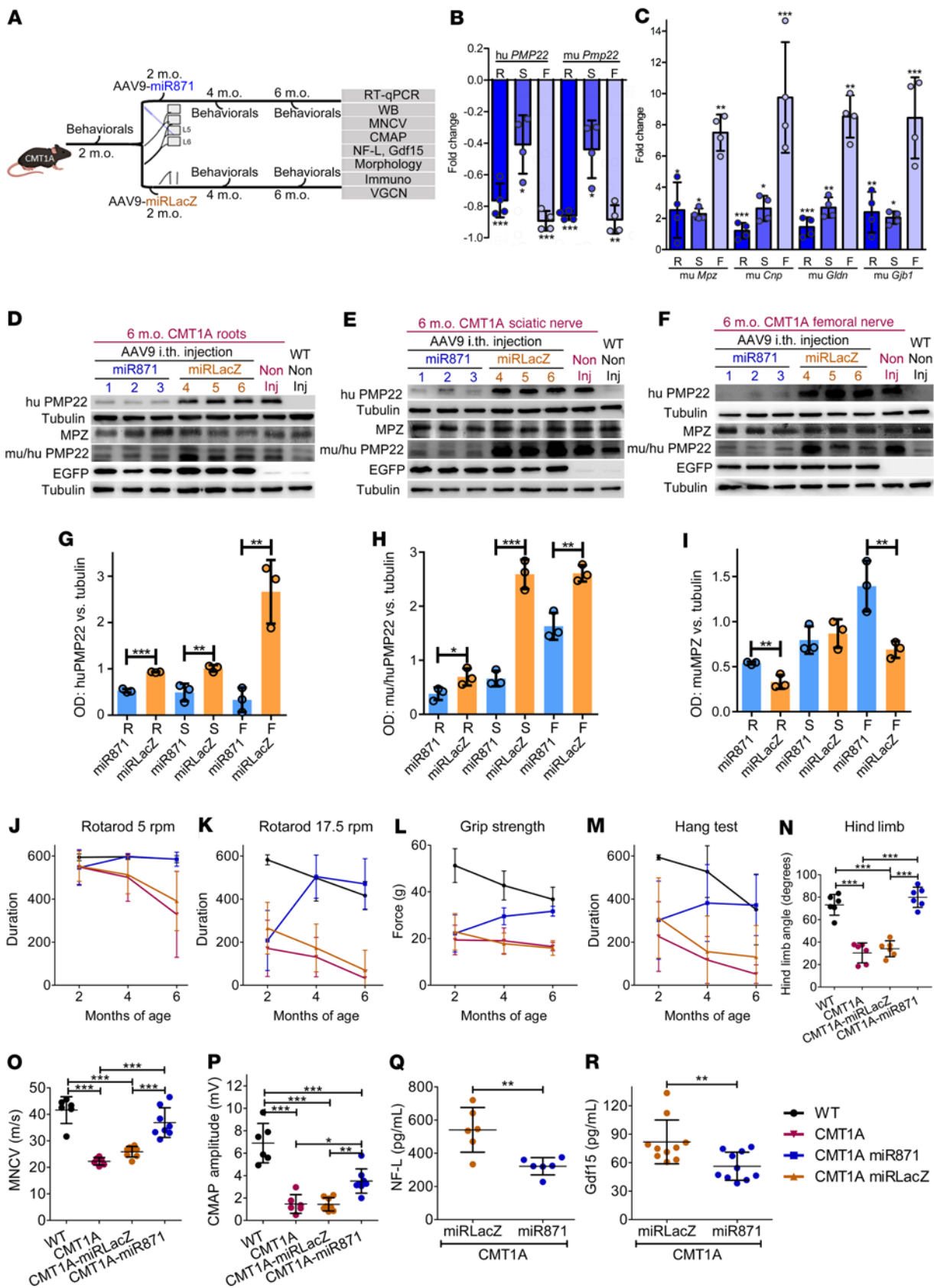


Figure 3. Efficient PMP22/Pmp22 silencing and improvement of motor behavioral, electrophysiological, and blood biomarker phenotypes following early treatment of CMT1A mice.

(A) Design of the early treatment trial. RT-qPCR analysis of (B) human *PMP22* and murine *Pmp22* and murine (C) *Mpz*, *Cnp*, *Gldn*, and *Gjb1* (C) gene expression levels in lumbar roots, sciatic nerves, and femoral nerves ($n = 4/\text{group}$). (D–I) Western blot images and analysis of human PMP22, murine PMP22, murine tubulin, EGFP, and murine MPZ proteins levels. (J–M) Behavioral analysis comparing noninjected WT and CMT1A mice ($n = 10/\text{group}$) and CMT1A-AAV9-miR871 and CMT1A-AAV9-miRLacZ mice ($n = 16/\text{group}$). (N) Hind limb opening angle estimation for 6-month-old noninjected WT and CMT1A mice ($n = 6/\text{group}$) as well as for CMT1A-AAV9-miR871 and CMT1A-AAV9-miRLacZ mice ($n = 6/\text{group}$). (O) MNCV and (P) CMAP analysis of 6-month-old WT and noninjected CMT1A mice ($n = 6/\text{group}$) and CMT1A-AAV9-miR871 and CMT1A-AAV9-miRLacZ mice ($n = 8/\text{group}$). (Q) NF-L ($n = 6/\text{group}$) and (R) Gdf15 ($n = 10/\text{group}$) circulating biomarker analysis of 6-month-old CMT1A-AAV9-miR871 and CMT1A-AAV9-miRLacZ mice. Values represent the mean \pm SD. * $P < 0.05$, ** $P < 0.01$, and *** $P < 0.001$, by unpaired, 1-tailed Student's *t* test (B, C, Q, and R) and 1-way ANOVA with Tukey's multiple-comparison test (G–P). For J–M, statistical significance is shown in Supplemental Figure 13.

of the AAV9-miRLacZ vector after injection into 2-months-old CMT1A mice that were examined 6 weeks (3.5 months of age) or 4 months (6 months of age) later. AAV9-miRLacZ caused no significant increase in the numbers of inflammatory cells in spinal roots, sciatic nerves, or dorsal root ganglia (DRGs) beyond the baseline (Supplemental Figures 8, 9, and 11). However, injection of AAV9-miRLacZ increased the number of CD20⁺ and CD3⁺ cells in CMT1A mouse livers 6 weeks after injection (3.5 months of age), but this reaction subsided by the 4-month post-injection time point (6 months of age; Supplemental Figure 10). Interestingly, inflammatory infiltrates increased with age in the PNS of noninjected CMT1A mice (Supplemental Figures 8 and 9).

After we confirmed sufficient biodistribution, transduction of PNS tissues, and safety, we evaluated the efficacy of AAV9-miR871 in silencing *PMP22/Pmp22* gene expression and reducing overall human and mouse PMP22 protein levels, compared with the expression of other myelin-related genes and proteins. We injected AAV9-miR871, which targets both the *PMP22* and *Pmp22* transcripts, or the AAV9-miRLacZ negative control, which expresses a functional but nontargeting miRNA, into adult CMT1A mice and then analyzed gene expression by RT-qPCR and Western blotting 6 weeks after injection. At the mRNA level, AAV9-miR871 downregulated *PMP22* and *Pmp22* in spinal roots and sciatic and femoral nerves, whereas other myelin-related genes were mostly elevated (Figure 2, D and E, and Supplemental Table 1). *Gjb1* transcript levels were increased in all tissues examined. *Mpz* and *Gldn* transcript levels were elevated only in roots, whereas *Cnp* transcript levels were elevated only in sciatic nerves. At the protein level (Figure 2, F–J), AAV9-miR871 selectively reduced human PMP22 levels in all PNS tissues examined (in roots: –66%, sciatic nerve: –86%, femoral nerve: –64%), whereas MPZ protein levels were increased in roots (by 23%) and femoral nerves (by 34%).

Early treatment of CMT1A mice. After validating AAV9-miR871 in vivo PNS biodistribution and *PMP22* and *Pmp22* gene silencing efficacy, we proceeded with a proof-of-concept treatment trial

at early stages of neuropathy in the CMT1A mouse model. Two-month-old CMT1A mice were injected with either AAV9-miR871 or AAV9-miRLacZ and evaluated 4 months after injection. For outcome analysis, we included *PMP22* and *Pmp22* expression levels using real-time PCR and Western blotting, behavioral testing, circulating neurofilament light (NF-L) and growth differentiation factor 15 (Gdf15) quantification, electrophysiological examination, as well as morphometric analysis of myelination in semithin sections and evaluation of inflammatory infiltrates in the PNS by IHC (Figures 3–5). We confirmed adequate biodistribution by VGCN measurement in PNS and non-PNS tissues as well as by immunofluorescence analysis in lumbar roots and sciatic nerves (Supplemental Figure 12).

At the mRNA level, early treatment with AAV9-miR871 in CMT1A mice (Figure 3A) downregulated *PMP22* and *Pmp22* in roots and sciatic and femoral nerves, while also elevating *Mpz*, *Cnp*, *Gldn*, and *Gjb1* transcripts levels (Figure 3, B and C, and Supplemental Table 2). At the protein level, early treatment with AAV9-miR871 in CMT1A mice reduced human and murine PMP22 levels in spinal roots (–43% human PMP22; –45% murine PMP22), sciatic nerves (–51% human PMP22; –74% murine PMP22), and femoral nerves (–87% human PMP22; –38% murine PMP22) (Figure 3, D–I). In contrast, we found that murine MPZ protein levels were increased in roots (63%) and femoral nerves (102%), reflecting improved myelination, whereas they remained unchanged in sciatic nerves (Figure 3, D–I).

We assessed motor performance in all groups before injection and until the end of the observation period by rotarod (5 and 17.5 rpm), grip, and hang tests (Figure 3, J–M, and Supplemental Figure 13). Time-course analysis of the above tests showed that AAV9-miR871 treatment improved the motor performance of CMT1A mice, reaching WT levels, whereas AAV9-miRLacZ-treated CMT1A mice performed similarly to noninjected CMT1A mice and significantly worse than WT mice (Figure 3, J–M, and Supplemental Figure 13). Moreover, early treatment with AAV9-miR871 completely rescued the hind limb clasping phenotype of CMT1A mice (Figure 3N and Supplemental Figure 14).

Electrophysiological examination in 6-month-old mice (4 months after vector injection) (Figure 3, O and P) showed a significantly improved MNCV score for AAV9-miR871-treated mice (36.87 ± 5.60 m/s) compared with that of the AAV9-miRLacZ-treated group (25.89 ± 1.99 m/s), approaching WT values at the same age (41.61 ± 5.06 m/s). Although the amplitude of the compound muscle action potential (CMAP) was also significantly improved in the treated mice (3.52 ± 1.08 mV) compared with AAV9-miRLacZ-treated controls (1.44 ± 0.59 mV), it did not reach WT levels (6.89 ± 1.76 mV).

As with other CMT blood biomarker studies, we found that circulating NF-L (76–79) and Gdf15 (80, 81) levels, associated with axonal degeneration, were significantly ameliorated after early treatment of CMT1A mice with AAV9-miR871 (NF-L: 321.37 ± 51.68 pg/mL; Gdf15: 56.25 ± 14.84 pg/mL) compared with their AAV9-miRLacZ vector-treated littermates (540.65 ± 134.49 pg/mL; Gdf15: 81.93 ± 23.12 pg/mL) (Figure 3, Q and R). This reduction in NF-L and Gdf15 levels in the AAV9-miR871 treatment group is consistent with improved motor function following gene-silencing treatment. Thus, NF-L and Gdf15 blood

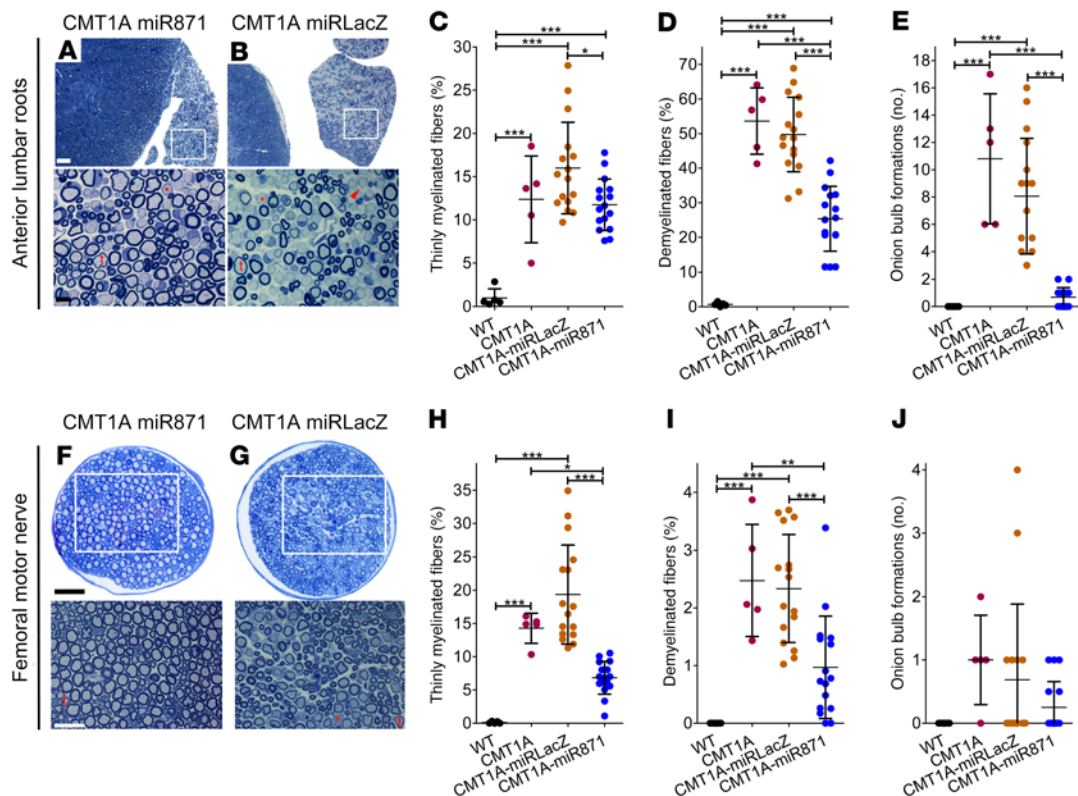


Figure 4. Early treatment of CMT1A mice improved PNS tissue morphology. Toluidine blue–stained semithin sections of (A and B) anterior lumbar spinal roots attached to the spinal cord and (F and G) femoral motor nerve at low (upper panels) and higher (lower panels) magnification from CMT1A-AAV9-miR871 and CMT1A-AAV9-miRLacZ mice. Thinly myelinated (t) or demyelinated (red asterisk) fibers as well as onion bulb formations (red arrowhead) are indicated. Quantification of abnormally myelinated fibers in (C–E) lumbar motor roots and (H–J) femoral motor nerves from 6-month-old noninjected WT and CMT1A mice ($n = 5/\text{group}$), as well as from CMT1A-AAV9-miR871 and CMT1A-AAV9-miRLacZ ($n = 16/\text{group}$). Values represent the mean \pm SD. * $P < 0.05$, ** $P < 0.01$, and *** $P < 0.001$, by 1-way ANOVA with Tukey's multiple-comparison test. Scale bars: (A and B) 50 μm and 10 μm (enlarged insets); (F and G) 40 μm and 25 μm (enlarged insets).

levels may be useful as treatment-responsive and clinically relevant biomarkers for future gene therapy in patients with CMT1A.

We performed morphometric analysis of myelination in transverse semithin sections of anterior lumbar roots and femoral motor nerves of 6-month-old CMT1A mice injected at the age of 2 months with either the AAV9-miR871 or the AAV9-miRLacZ vector. We examined multiple roots and bilateral femoral motor nerves from each mouse and calculated the percentage of thinly myelinated and demyelinated fibers, as well as the number of onion bulb formations. In both roots (Figure 4, A–E) and femoral nerves (Figure 4, F–J), the percentage of thinly myelinated and demyelinated fibers was significantly reduced in the treated mice. Spinal roots also showed reduced numbers of onion bulb formations, whereas femoral onion bulb formations were already low at baseline and not altered after treatment. The degree of myelin pathology was too mild in the sciatic nerves of CMT1A mice to be considered as a treatment readout (Supplemental Figure 15).

Finally, for this early treatment group, we used immunofluorescence analysis to evaluate the inflammatory status of lumbar roots and sciatic nerves (Figure 5 and Supplemental Figures 16–18). AAV9-miR871 treatment decreased the percentage of CD20⁺, CD45⁺, CD68⁺, and CD3⁺ cells. Moreover, injection

with the therapeutic vector did not cause any inflammatory responses in the liver at the 4-month post-injection point (Supplemental Figure 18).

Late treatment compared with extended early treatment. After assessing the effectiveness of early treatment with AAV9-miR871 in CMT1A mice, we further examined its effectiveness when injected later in the disease course. We injected mice either at 6 months (late treatment) or 2 months (extended early treatment) of age and analyzed various outcomes at 10 months of age. We evaluated both mice that received late treatment (4 months after injection) and mice that were had extended early treatment (8 months after injection) using a VGCN calculation, behavioral testing, blood NF-L and Gdf15 testing, electrophysiological examination, as well as by morphometric analysis of myelination and IHC, while real-time PCR and Western blot analysis were performed only in the late treatment groups (Figure 6A). Vector biodistribution in older animals was confirmed by VGCN in PNS and non-PNS tissues (Supplemental Figures 19A and 20). In the late treatment group, we confirmed vector biodistribution with EGFP expression levels in lumbar roots and sciatic nerves (Supplemental Figure 19B).

At the mRNA level, as with early treatment, late treatment with AAV9-miR871 in CMT1A mice downregulated *PMP22* and

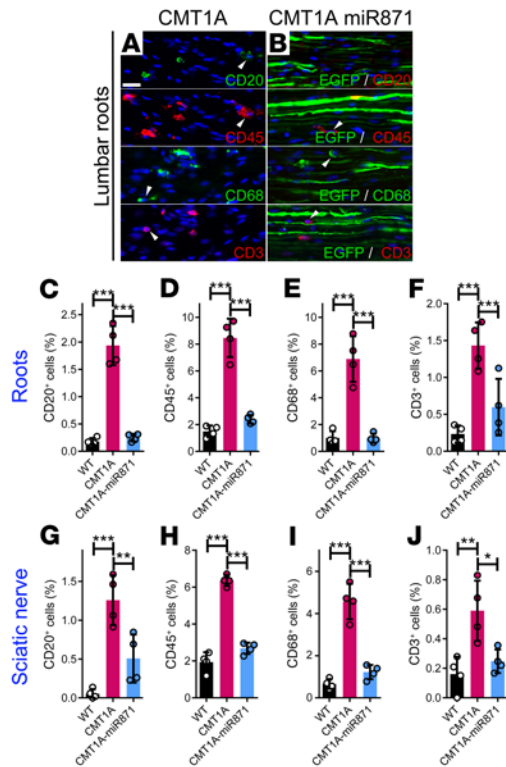


Figure 5. Early treatment of CMT1A mice improved inflammation in PNS tissues. Images of longitudinal lumbar spinal root sections from noninjected CMT1A mice and mice that received early treatment with CMT1A-AAV9-miR871. Root sections were immunostained for CD20, CD45, CD68, and CD3 markers (A and B). The injected tissues were counterstained with the nuclear marker DAPI (blue) and EGFP (green) autofluorescence. Arrowheads indicate representative CD⁺ cells. Quantification of the percentage of inflammatory cells in lumbar roots (C–F) and sciatic nerve (G–J). Values represent the mean \pm SD ($n = 4$ /group). * $P < 0.05$, ** $P < 0.01$, and *** $P < 0.001$, by 1-way ANOVA with Tukey’s multiple-comparison test followed by Bonferroni’s correction. Scale bar: 20 μ m. (WT and CMT1A immunostained images and quantification data are also shown in Supplemental Figures 8 and 9.)

Pmp22, while also elevating *Mpz*, *Cnp*, *Gldn*, and *Gjb1* transcripts levels in roots and sciatic and femoral nerves (Figure 6, B and C, and Supplemental Table 3). At the protein level, late treatment with AAV9-miR871 reduced human and murine PMP22 levels in all PNS tissue samples examined (Figure 6, D–I). In contrast, murine MPZ protein levels were increased in roots and femoral nerves, reflecting improved myelination, but remained unchanged in sciatic nerves (Figure 6, D–I).

We compared motor performance of mice in the late treatment group with that of mice in the extended early treatment group and of age-matched, noninjected WT and CMT1A mice (Figure 6, J–N, and Supplemental Figures 21 and 22). We evaluated all groups before injection and until the end of the observation period by rotarod (5 rpm and 17.5 rpm), grip strength, and hang test analyses (Figure 6, J–M). Time-course analysis of the above tests showed that CMT1A mice that received late or extended early AAV9-miR871 treatment performed similarly, reaching WT levels, whereas CMT1A mice that received

AAV9-miRLacZ late treatment performed similarly to noninjected CMT1A mice and significantly worse than WT mice (Figure 6, J–M, and Supplemental Figures 21 and 22). AAV9-miR871 late treatment improved the hind limb clasping phenotype of CMT1A mice, but without reaching WT levels, in contrast to mice given the extended early treatment, in which the phenotype was completely rescued, reaching WT levels (Figure 6N and Supplemental Figure 23).

Electrophysiological examination of 10-month-old mice showed that the sciatic MNCV was significantly improved in CMT1A mice in both the late (36.92 ± 3.94 m/s) and extended early (38.74 ± 5.30 m/s) AAV9-miR871 treatment groups compared with the AAV9-miRLacZ-treated group (24.82 ± 2.58 m/s) (Figure 6O). Interestingly, only the CMT1A mice that received extended early treatment reached age-matched WT values (43.50 ± 2.72 m/s). CMAP amplitudes were not improved in any of the AAV9-miR871 treatment groups (Figure 6P). Similarly, NF-L and Gdf15 levels remained elevated in the animals that were treated late compared with age-matched WT mice (Figure 6, Q and R).

We performed morphometric analysis of myelination in transverse semithin sections of PNS tissues from 10-month-old CMT1A mice that received late or extended early treatment. With this analysis, we showed that the anterior lumbar roots (Figure 7, A–F) and femoral motor nerves (Figure 7, G–L) had significantly reduced percentages of thinly myelinated and demyelinated fibers in the mice that received late treatment, but without reaching WT levels. In contrast, these morphological abnormalities were fully rescued in the mice that underwent extended early treatment, reaching WT levels (Figure 7, A–L). The degree of myelin pathology remained too mild in the sciatic nerves of 10-month-old CMT1A mice to be considered as a treatment readout (Supplemental Figure 24).

As in the early treatment group, analysis of inflammation by immunofluorescence revealed that late treatment with AAV9-miR871 decreased the numbers of CD20⁺, CD45⁺, CD68⁺, and CD3⁺ cells in PNS tissues (Figure 8 and Supplemental Figures 25 and 26). Injection with the therapeutic vector did not cause any inflammatory responses in the liver 4 months after injection (Supplemental Figure 27).

Discussion

CMT1A is the most common inherited demyelinating neuropathy, resulting from a *PMP22* gene dosage effect in SCs. Ideally, CMT1A therapies should reduce overexpressed *PMP22*, while avoiding excessive knockdown that could lead to the milder phenotype of hereditary neuropathy with pressure palsies (HNPP). We accomplished that here with our study, which, to our knowledge, presents the first translatable AAV9-mediated *PMP22* gene-silencing approach leading to phenotypic improvement in a CMT1A mouse model. Although this is a preclinical study, we designed our approach from the outset with an eye toward translation to prospective human clinical trials, in 2 ways. First, the therapeutic construct is applicable to animal models and patients with CMT1A alike. The most relevant animal models, such as the C61-het mouse we used here, express transgenic copies of human *PMP22* on a normal mouse background. Thus, both murine *Pmp22* and human *PMP22* genes contribute to

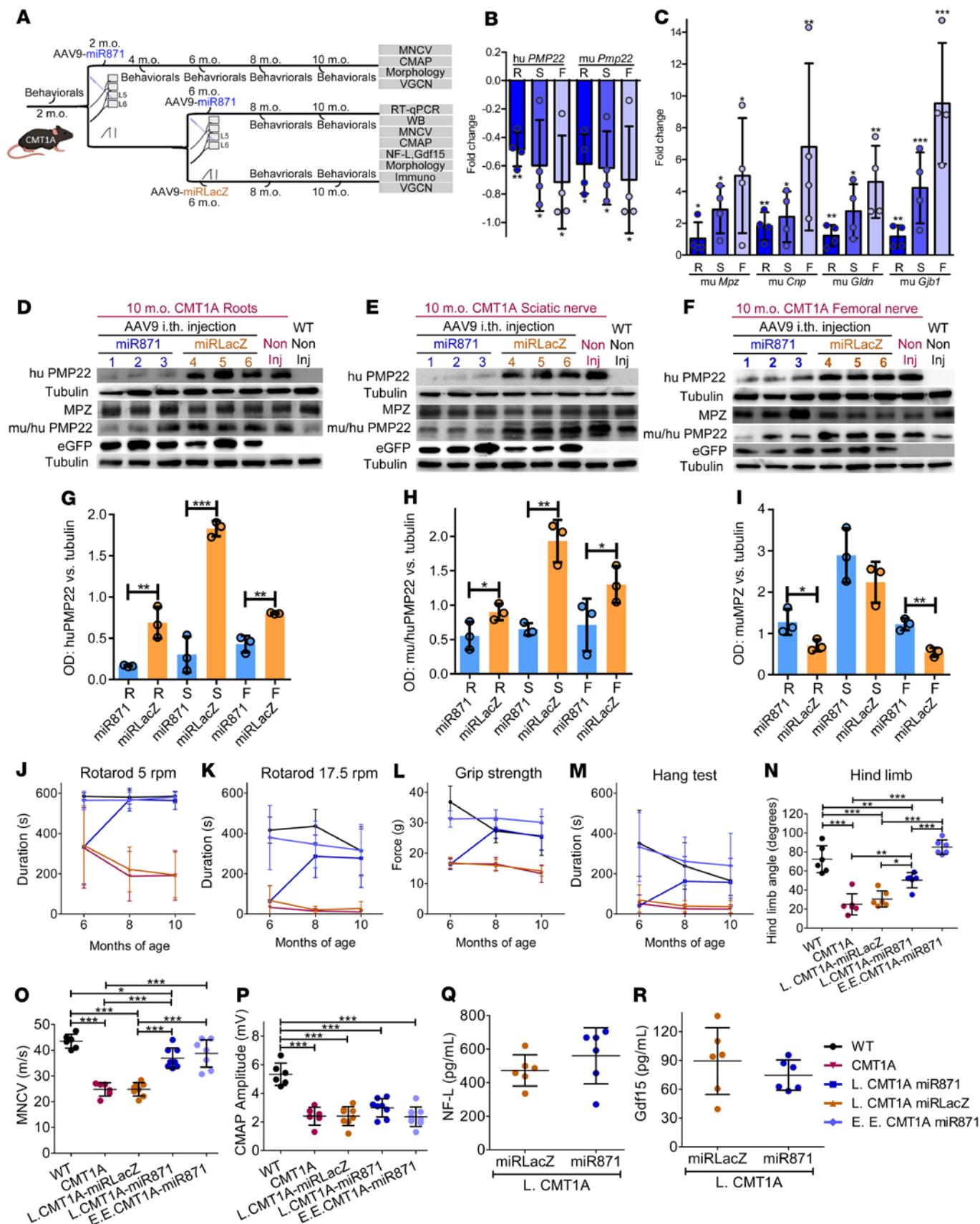


Figure 6. Efficient PMP22/Pmp22 silencing and improvement of motor function and sciatic MNCVs but not CMAPs or blood biomarker phenotypes following late treatment of CMT1A mice. (A) Design of the late (L.) and extended early (E.E.) treatment trial. RT-qPCR analysis of (B) *PMP22* and *Pmp22* and (C) *Mpz*, *Cnp*, *Gldn*, and *Gjb1* gene expression in lumbar roots and sciatic and femoral nerves of late-treated CMT1A mice ($n = 4/\text{group}$). (D–I) Western blots and analysis of human PMP22, murine PMP22, murine tubulin, EGFP, and murine MPZ protein levels. (J–M) Behavioral analysis comparing noninjected WT and CMT1A mice ($n = 10/\text{group}$) and CMT1A-AAV9-miR871 and CMT1A-AAV9-miR-LacZ mice ($n = 16/\text{group}$). (N) Hind limb opening angle estimation for 10-month-old noninjected WT and CMT1A mice ($n = 6/\text{group}$) and L.CMT1A-AAV9-miR871, E.E.CMT1A-AAV9-miR871, and CMT1A-AAV9-miRLacZ mice ($n = 6/\text{group}$). (O) MNCV and (P) CMAP analysis of 10-month-old WT and noninjected CMT1A mice ($n = 6/\text{group}$) and L.CMT1A-AAV9-miR871, E.E.CMT1A-AAV9-miR871, and CMT1A-AAV9-miRLacZ mice ($n = 8/\text{group}$). (Q) NF-L ($n = 6/\text{group}$) and (R) Gdf15 ($n = 10/\text{group}$) circulating biomarker analysis in 10-month-old L.CMT1A-AAV9-miR871 and L.CMT1A-AAV9-miRLacZ mice. Values represent the mean \pm SD. * $P < 0.05$, ** $P < 0.01$, and *** $P < 0.001$, by unpaired, 1-tailed Student's *t* test (B, C, Q, and R) and 1-way ANOVA with Tukey's multiple-comparison test (G–P). For J–M, statistical significance is shown in Supplemental Figures 21 and 22.

excessive gene dosage, leading to CMT1A-like phenotypes, and testing a translatable approach in mice requires targeting both transcripts. Importantly, the artificial miRNA we designed, miR871, targets both human *PMP22* and murine *Pmp22* transcripts. Second, we delivered AAV9-miR871 through a clinically applicable method of lumbar intrathecal injection into C61-het CMT1A mice, which reproduces the clinical course, severity, and symptoms of patients with CMT1A.

The translatability and effectiveness of the intrathecal administration route have been demonstrated in larger animals (82, 83) and in human trials (NCT03381729, NCT02362438), which showed effects in nerves distal to the injection site, including transduction of SCs in the tibial nerve of dogs after intrathecal injection of AAV9 (83). Another route of administration that could be easily translated to the clinic is intravenous injections. However, our studies in mice showed that intrathecal injection provides adequate biodistribution throughout the PNS, with much lower vector amounts injected compared with intravenous delivery (84). Intraneural injections of AAV-shRNA were also proposed to treat a CMT1A model (73), however, the translatability of this delivery method is considered challenging in the clinic.

In addition to incorporating species conservation and a feasible route of administration into our study design, we also demonstrated efficacy at multiple levels. First, we confirmed in vitro and in vivo the *PMP22/Pmp22* silencing efficiency of miR871 and its effects on other myelin-related genes and proteins, while also assessing the transduction efficiency of AAV9 in PNS tissues after lumbar intrathecal injection (Figures 1 and 2). We then demonstrated by multiple outcome measures the therapeutic effects of AAV9-miR871 after treatment at both early and later stages of the neuropathy, supporting the relevance of this approach for direct clinical translation to treat CMT1A. As demonstrated through our detailed baseline longitudinal, functional, and morphological analyses, the C61 het

model of CMT1A used in this study develops an early-onset, progressive demyelinating pathology that reproduces human disease features (Supplemental Figures 2–7). Thus, already at the early intervention time point, the model presented significant pathological features and slowing of nerve conduction velocities that progressed with aging. Therefore, both early and late treatments represent post-onset interventions, reproducing the clinical scenario of treating younger or older patients with CMT1A, in whom demyelination is already present in childhood (85, 86), followed by slowly progressive axonal loss (8, 9, 87, 88). Our mouse data suggest that earlier treatment is effective, as several outcome measures were corrected to WT levels (Figures 3–5). A direct comparison of CMT1A mice that received extended early or late treatment, injected at 2 or 6 months of age, respectively, and analyzed at 10 months of age, confirmed that treatment more efficiently reversed disease manifestations if given earlier (Figures 6 and 7). This could be explained by the fact that later stages of the neuropathy were characterized by already advanced axonal degeneration. While it appears feasible to stimulate remyelination by transduced demyelinating SCs, increasing axonal loss found at later stages is irreversible. Nevertheless, our data suggest that the ability to improve CMT1A-like symptoms in mice with preexisting pathology is promising for the translation of this strategy to patients who may already be experiencing the effects of CMT1A. Indeed, our work is consistent with the findings of a tetracycline-inducible *Pmp22*-transgenic mouse study (89). *Pmp22* overexpression occurred in the absence of tetracycline, causing demyelination and numerous neuropathic phenotypes. Importantly, when mice were given tetracycline, thereby shutting off the *Pmp22* transgene, myelin normalization began to occur within 1 week, with nearly normal myelin observed by 4 months. Together, these data and ours suggest that some CMT1A phenotypes may be reversible. It is also possible that we will see an even greater reversal of phenotypes in these mice as they age 4 months after treatment.

Another question we considered, regarding translation, was the necessity to restrict miR871 expression to SCs alone. In our previous studies (84), we demonstrated that an AAV9 vector expressing a transgene through the SC-specific *Mpz* promoter efficiently transduced myelinating SCs throughout the PNS following a single lumbar intrathecal injection. In the current study, we used AAV9 to deliver a U6.miR.CMV.EGFP construct, in which both sequences (EGFP and miR871) were driven by ubiquitous promoters (CMV and U6, respectively) (Figure 1D). We calculated transduction rates via immunofluorescence using the CMV.EGFP reporter gene and VGCN analysis (Figure 2). Not surprisingly, expression was more widespread, with both SCs and other cell types transduced, including motor and sensory neurons, leading to axonal expression. We also detected VGCNs in many non-PNS tissues typically transduced by AAV9, with the highest numbers detected in the liver (Supplemental Figures 12 and 19), but without any apparent toxic effects in lumbar roots, sciatic nerves, liver, or DRGs (Figures 5 and 8, and Supplemental Figures 8–11, 16–18, and 25–27). Given that *PMP22* expression levels are normally very low and do not have any known effects in other cell types besides myelinating SCs

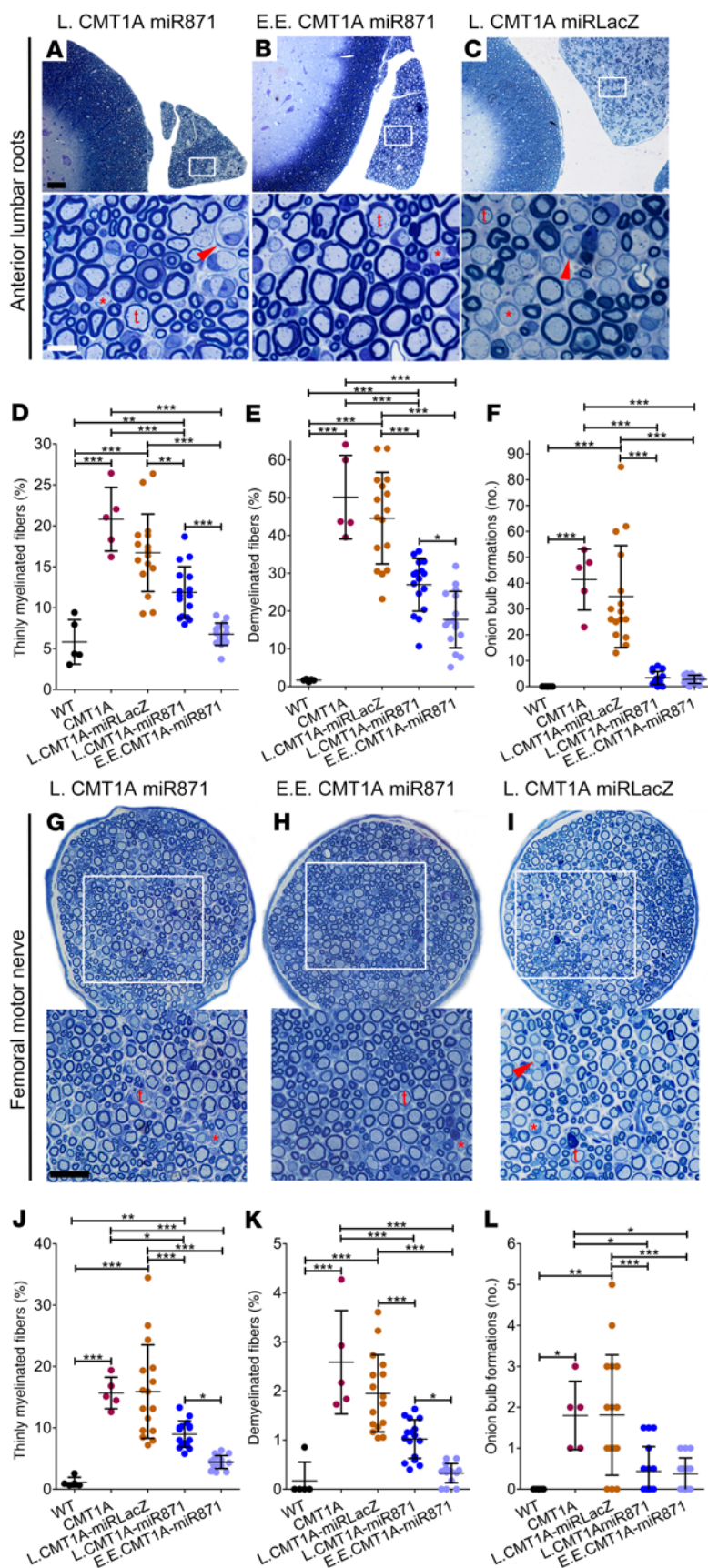


Figure 7. Late and extended early treatment of CMT1A mice improved PNS tissue morphology. Toluidine blue-stained semithin sections of (A–C) anterior lumbar spinal roots attached to the spinal cord and (G–I) femoral motor nerves (at low and higher magnification) from 10-month-old L.CMT1A-AAV9-miR871, E.E.CMT1A-AAV9-miR871, and L.CMT1A-AAV9-miRLacZ mice. Thinly myelinated (t) and demyelinated (red asterisk) fibers as well as onion bulb formations (red arrowhead) are indicated. (D–F) Quantification of abnormally myelinated fibers and onion bulb formations in multiple roots, and (J–L) femoral motor nerves from 10-month-old WT and noninjected CMT1A ($n = 5/\text{group}$) mice and L.CMT1A-AAV9-miR871, E.E.CMT1A-AAV9-miR871, and L.CMT1A-AAV9-miRLacZ mice ($n = 16/\text{group}$). Values represent the mean \pm SD. * $P < 0.05$, ** $P < 0.01$, and *** $P < 0.001$, by 1-way ANOVA with Tukey’s multiple-comparison test. Scale bars: (A–C) 50 μm and 10 μm (enlarged insets); (G–I) 40 μm and 25 μm (enlarged insets).

(11, 90–92), we do not expect any adverse effects from ubiquitous silencing of PMP22 expression. It is also important to mention that transduction evaluation through a reporter gene may not directly correlate with miR expression, when using 2 different ubiquitous promoters. An emerging area of study involves the ability of miRs to travel outside transduced cells through exosomes and potentially act at distant sites and neighboring cells. We did not directly measure exosome packaging of miR871, but future work should determine the potential for incomplete transduction leading to broader correction in adjacent, nontransduced cells.

The 5e11 vg/mouse vector dose used for intrathecal injection in this study corresponds to approximately 2.3e13 vg/kg. With this dose, we achieved sufficient SC transduction and PMP22 silencing to improve molecular, histopathological, and functional deficits. As such, this dose is comparable to those used in prior clinical AAV9 gene therapy studies that targeted motor neurons in the spinal cord, including the Avexis SMA trial (NCT03381729) for intrathecal delivery of Zolgensma 1.2e13vg/kg (93) and the giant axonal neuropathy (GAN) clinical trial (NCT02362438), in which intrathecal doses ranged from 3.5×10^{13} to 3.5×10^{15} total vg/patient ($\sim 1.75 \times 10^{12}$ vg/kg to 1.75×10^{13} vg/kg) (94). Given that our dose was slightly higher than those currently used in clinical trials and the fact that our potential treatment population would be mostly adults with CMT1A, a dose escalation study would be useful for identifying the optimal vector concentration that would provide robust therapeutic benefit and minimal risk of PMP22 haploinsufficiency.

To examine the potential side effects of PMP22/Pmp22 oversilencing, we tested AAV9-miR871 in WT mice (Supplemental Results and Supplemental Figures

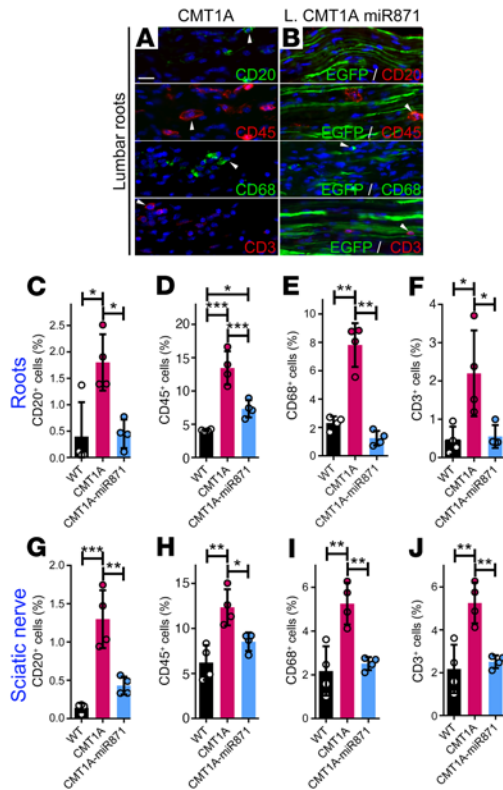


Figure 8. Late treatment of CMT1A mice improved inflammation in PNS tissues. Images of longitudinal lumbar spinal root sections from noninjected and late-treated CMT1A-AAV9-miR871 mice immunostained for CD20, CD45, CD68, and CD3 markers (A and B). The injected tissues were counterstained with the nuclear marker DAPI (blue) and EGFP (green) autofluorescence. Arrowheads indicate representative CD⁺ cells. Quantification of the percentage of inflammatory cells in lumbar roots (C–F) and sciatic nerves (G–J). Values represent the mean \pm SD ($n = 4$ /group). * $P < 0.05$, ** $P < 0.01$, and *** $P < 0.001$, by 1-way ANOVA with Tukey's multiple-comparison test. Scale bar: 20 μ m (immunostained images are also shown in Supplemental Figure 25).

28–34). Despite muPmp22 levels being significantly reduced in WT-injected mice, we found only mild functional and electrophysiological abnormalities without the typical HNPP-like phenotype (95). Since our treatment is not intended to be applied to individuals with normal levels of PMP22 expression, the partial phenotype observed in WT mice based on the dual human-murine targeting capacity of miR871 does not raise safety concerns regarding the potential treatment of patients with CMT1A. This set of experiments in WT mice also underscores the importance of targeting all sources of *PMP22/Pmp22* in an animal model, especially when performing dose-finding studies to determine potential clinical doses.

Several therapeutic approaches for CMT1A have been suggested so far (61, 68), with the most clinically advanced being oral PXT3003. Although PXT3003 was shown to improve the symptoms of CMT1A in rats (56) and humans (60), its *Pmp22*-silencing efficiency was shown only at the mRNA level in the rat overexpressing murine *Pmp22*. It is still unclear how PXT3003 affects human PMP22. Although other pharmacological treatments have been suggested through the years, most of them are

symptomatic, require repeated treatment sessions, or have potential long-term side effects. For example, intravenously delivered squalenoyl siRNA PMP22 nanoparticles (67) have been shown to provide therapeutic benefit in JP18/JY13 mice overexpressing the human *PMP22* gene. However, potential toxicity with repeated dosing and long-term stability, as well as the effects of this treatment on *PMP22* mRNA or protein levels, remain to be shown. On the contrary, a gene therapy approach like ours would provide a one-off treatment option. In a previously reported preclinical gene therapy approach, AAV2/9 vectors expressed shRNAs specifically designed to target murine *Pmp22* (73). Because the shRNAs contain potentially disruptive mismatches with the human transcript, their direct translatability in humans was untested and remains unclear. Moreover, the shRNA vectors were delivered through direct intraneural injection, a method that is more difficult to translate to clinical practice for treating CMT1A and carries more risks because of the toxic nature of concentrated anesthesia and the risk of direct fiber damage (96). In contrast, the lumbar intrathecal injection used in our study is considered a routine procedure that can be easily applied in the clinic, providing widespread biodistribution in the PNS. Compared with intravenous delivery, intrathecal delivery also requires a much lower viral volume to provide beneficial effects and hence results in lower toxicity (84, 97). It remains to be shown that adequate biodistribution can also be achieved in larger animals before clinical translation.

Regarding the safety of AAV9-based vectors in humans, follow-up studies in AAV9-treated patients with spinal muscular atrophy (SMA) suggested stable beneficial effects of Zolgensma with no major adverse reactions or long-term toxicity (93, 98, 99). However, more recent studies suggest that long-term overexpression of proteins (100) or miRNAs (101) via AAV9 viral vectors may dysregulate endogenous mechanisms, causing toxic side effects. Our data suggested that AAV9-miR871 treatment did not cause inflammation in PNS tissues, as had been previously suggested in another study using the AAV9 serotype carrying a different payload (102), but in fact acted to reduce inflammation native to the CMT1A animal model. Moreover, injection with the therapeutic vector did not cause any chronic inflammatory responses in the liver 4 months after injection (Supplemental Figures 18 and 27). Although our approach was shown to improve the baseline inflammatory status of the CMT1A model without causing any systemic or liver toxicity, it will be important to consistently demonstrate its safety with more detailed toxicity studies across different species. Potential cellular and humoral immune responses can be stimulated against the AAV capsid or protein-coding gene product. Since our one-off therapeutic payload is a noncoding RNA, our vector should be inherently less immunogenic than those used in gene replacement strategies.

To design successful clinical trials involving patients with CMT1A, it is important to establish relevant and sensitive outcome measures. The gene-silencing approach described here provides functional improvements that can be easily evaluated in patients through electrophysiological testing. Since previous clinical trials suggested a lack of sensitivity of standard CMT clinical scores to detect treatment response (45, 103), more detailed clinical functional and patient-reported outcome measures will also be necessary (104–107), along with MRI-based quantification of

muscle atrophy (108). Here, we also demonstrate, for the first time to our knowledge, the responsiveness of NF-L (109, 110) and Gdf15 (80, 81) plasma biomarkers in a CMT1A model. Responsiveness of these translatable biomarkers is highly encouraging for their utility in parallel clinical trials of miRNA therapies. Although, a recent study (79) showed a lack of correlation of NF-L plasma levels with disease progression over time in patients with CMT1A, this might be due to the older age of the patients tested (mean age, 46 years). In this regard, validation of additional clinically relevant plasma and skin biomarkers as indicators for future gene therapy efficacy would be essential (19, 111, 112, 113).

In conclusion, we developed and characterized an artificial miRNA designed to specifically target human *PMP22* and murine *Pmp22* transcripts and evaluated the therapeutic benefit in a CMT1A mouse model that reproduces CMT1A-associated phenotypes. Our results indicate that a single lumbar intrathecal injection of AAV9-miR871 at early and late stages of the neuropathy, and always after onset, can correct the functional, morphological, and inflammatory abnormalities of CMT1A without causing any apparent side effects. Taken together, these results constitute an important step toward the development of a clinically relevant and translatable gene therapy to treat CMT1A.

Methods

All materials and methods are presented in the Supplemental Methods.

Statistics. Each set of data is presented as the mean \pm SD or SEM, with *n* equal to the number of biological repeats for in vitro experiments or independent samples from individual animals for in vivo experiments. For comparison of means between 2 independent groups, an unpaired, 1-tailed Student's *t* test was performed. For comparison of means between 3 or more independent groups, 1-way ANOVA was performed. Statistical significance for all experiments was defined as a *P* value of less than 0.05. When ANOVA tests suggested significant difference among groups, Tukey's multiple-comparison post hoc test was applied. When a sample group was used for more than 1 comparison, Bonferroni's correction of *P* values was additionally applied. All statistical analyses were performed using GraphPad Prism, version 6 (GraphPad Software).

Study approval. All animal procedures were approved by the Cyprus Government's chief veterinary officer (project license CY/EXP/PR.L3/2017) according to national law, which is harmonized with European Union guidelines (EC Directive 86/609/EEC).

Author contributions

MS co-designed and conducted or directed all experiments, acquired and analyzed data, created figures and legends, and drafted and reviewed the manuscript. AK performed electrophysiology experiments. SGC performed and analyzed in vitro screening of artificial miRNAs. MJJ and RH standardized, performed and analyzed ELISAs for serum Gdf15 levels. LMW contributed to in vitro screening of artificial miRNAs. AMF assisted with viral vector production. AH and HZ performed and analyzed plasma NF-L levels. JR, CT, and CC performed and analyzed VGCNs. SQH designed artificial miRNAs and supervised in vitro screening, created figures and legends, and drafted and reviewed the manuscript. KAK co-designed and supervised all experiments and drafted and reviewed the manuscript. All authors read and approved the final manuscript.

Acknowledgments

We thank members of Andelyn Biosciences (formerly the Viral Vector Core at Nationwide Children's Hospital) for producing the AAV9 virus used in this study and Nettie Pyne for molecular biology assistance. We would also like to extend our gratitude to Rudolf Martini for providing C61 het breeding pairs to establish and expand the colony at The Cyprus Institute of Neurology and Genetic. This work was funded by a grant from the CMT Research Foundation. HZ was funded by the UK Dementia Research Institute (UKDRI-1003) and the Wellcome Trust. HZ is a Wallenberg Scholar. RH is a Wellcome Trust Investigator (109915/Z/15/Z), who receives support from the Medical Research Council (UK) (MR/N025431/1 and MR/V009346/1), the Addenbrookes Charitable Trust (G100142), the Evelyn Trust, the Stoneygate Trust, the Lily Foundation, and an MRC strategic award to establish an International Centre for Genomic Medicine in Neuromuscular Diseases (ICGNMD) MR/S005021/1. MJJ is supported by the Medical Research Council (MRC) (UK) DiMeN and Cambridge DTPs. This research was supported by the National Institute for Health and Care Research (NIHR) Cambridge Biomedical Research Centre (BRC-1215-20014). The views expressed are those of the authors and not necessarily those of the NIHR or the Department of Health and Social Care.

Address correspondence to: Kleopas A. Kleopa, The Cyprus Institute of Neurology and Genetics, 6 Iroon Avenue, P.O. Box 23462, 1683, Nicosia, Cyprus. Phone: 357.22.358600; Email: kleopa@cing.ac.cy.

- Skre H. Genetic and clinical aspects of Charcot-Marie-Tooth's disease. *Clin Genet.* 1974;6(2):98-118.
- Martyn CN, et al. Epidemiology of peripheral neuropathy. *J Neurol Neurosurg Psychiatry.* 1997;62(4):310-318.
- Lupski JR, et al. DNA duplication associated with Charcot-Marie-Tooth disease type 1A. *Cell.* 1991;66(2):219-232.
- Matsunami N, et al. Peripheral myelin protein-22 gene maps in the duplication in chromosome 17p11.2 associated with Charcot-Marie-Tooth 1A. *Nat Genet.* 1992;1(3):176-179.
- Patel PI, et al. The gene for the peripheral myelin protein PMP-22 is a candidate for Charcot-Marie-Tooth disease type 1A. *Nat Genet.* 1992;1(3):159-165.
- Timmerman V, et al. The peripheral myelin protein gene PMP-22 is contained within the Charcot-Marie-Tooth disease type 1A duplication. *Nat Genet.* 1992;1(3):171-175.
- Valentijn LJ, et al. The peripheral myelin gene PMP-22/GAS-3 is duplicated in Charcot-Marie-Tooth disease type 1A. *Nat Genet.* 1992;1(3):166-170.
- Thomas PK, et al. The phenotypic manifestations of chromosome 17p11.2 duplication. *Brain.* 1997;120(pt 3):465-478.
- Krajewski KM, et al. Neurological dysfunction and axonal degeneration in Charcot-Marie-Tooth disease type 1A. *Brain.* 2000;123(pt 7):1516-1527.
- Snipes GJ, et al. Characterization of a novel peripheral nervous system myelin protein (PMP-22/SR13). *J Cell Biol.* 1992;117(1):225-238.
- Notterpek L, et al. Peripheral myelin protein 22 is a constituent of intercellular junctions in epithelia. *Proc Natl Acad Sci U S A.* 2001;98(25):14404-14409.
- Adlkofer K, et al. Hypermyelination and demyelinating peripheral neuropathy in Pmp22-deficient mice. *Nat Genet.* 1995;11(3):274-280.
- Adlkofer K, et al. Heterozygous peripheral myelin protein 22-deficient mice are affected by a progressive demyelinating tomaculous neuropathy. *J Neurosci.* 1997;17(12):4662-4671.
- Suh JG, et al. An in-frame deletion in peripheral myelin protein-22 gene causes hypomyelination and cell death of the Schwann cells in the new Trembler mutant mice. *Neuroscience.*

- 1997;79(3):735-744.
15. Fledrich R, et al. Soluble neuregulin-1 modulates disease pathogenesis in rodent models of Charcot-Marie-Tooth disease 1A. *Nat Med.* 2014;20(9):1055-1061.
 16. Roa BB, et al. Molecular basis of Charcot-Marie-Tooth disease type 1A: gene dosage as a novel mechanism for a common autosomal dominant condition. *Am J Med Sci.* 1993;306(3):177-184.
 17. Yoshikawa H, et al. Elevated expression of messenger RNA for peripheral myelin protein 22 in biopsied peripheral nerves of patients with Charcot-Marie-Tooth disease type 1A. *Ann Neurol.* 1994;35(4):445-450.
 18. Vallat JM, et al. Ultrastructural PMP22 expression in inherited demyelinating neuropathies. *Ann Neurol.* 1996;39(6):813-817.
 19. Svaren J, et al. Schwann cell transcript biomarkers for hereditary neuropathy skin biopsies. *Ann Neurol.* 2019;85(6):887-898.
 20. Sereda M, et al. A transgenic rat model of Charcot-Marie-Tooth disease. *Neuron.* 1996;16(5):1049-1060.
 21. Huxley C, et al. Construction of a mouse model of Charcot-Marie-Tooth disease type 1A by pronuclear injection of human YAC DNA. *Hum Mol Genet.* 1996;5(5):563-569.
 22. Huxley C, et al. Correlation between varying levels of PMP22 expression and the degree of demyelination and reduction in nerve conduction velocity in transgenic mice. *Hum Mol Genet.* 1998;7(3):449-458.
 23. Robertson AM, et al. Development of early postnatal peripheral nerve abnormalities in Trembler-J and PMP22 transgenic mice. *J Anat.* 1999;195(pt 3):331-339.
 24. Norreel JC, et al. Behavioural profiling of a murine Charcot-Marie-Tooth disease type 1A model. *Eur J Neurosci.* 2001;13(8):1625-1634.
 25. Robaglia-Schlupp A, et al. PMP22 overexpression causes dysmyelination in mice. *Brain.* 2002;125(pt 10):2213-2221.
 26. Sereda MW, et al. Animal models of Charcot-Marie-Tooth disease type 1A. *Neuromolecular Med.* 2006;8(1-2):205-216.
 27. Verhamme C, et al. Myelin and axon pathology in a long-term study of PMP22-overexpressing mice. *J Neuropathol Exp Neurol.* 2011;70(5):386-398.
 28. Fledrich R, et al. Murine therapeutic models for Charcot-Marie-Tooth (CMT) disease. *Br Med Bull.* 2012;102:89-113.
 29. Jouaud M, et al. Rodent models with expression of PMP22: Relevance to dysmyelinating CMT and HNPP. *J Neurol Sci.* 2019;398:79-90.
 30. Bosco L, et al. Animal models as a tool to design therapeutic strategies for CMT-like hereditary neuropathies. *Brain Sci.* 2021;11(9):1237.
 31. Pareek S, et al. Neurons promote the translocation of peripheral myelin protein 22 into myelin. *J Neurosci.* 1997;17(20):7754-7762.
 32. Notterpek L, et al. PMP22 accumulation in aggresomes: implications for CMT1A pathology. *Neurobiol Dis.* 1999;6(5):450-460.
 33. Ryan MC, et al. Aggresome formation in neuropathy models based on peripheral myelin protein 22 mutations. *Neurobiol Dis.* 2002;10(2):109-118.
 34. Fortun J, et al. Impaired proteasome activity and accumulation of ubiquitinated substrates in a hereditary neuropathy model. *J Neurochem.* 2005;92(6):1531-1541.
 35. Sahenk Z, et al. NT-3 promotes nerve regeneration and sensory improvement in CMT1A mouse models and in patients. *Neurology.* 2005;65(5):681-689.
 36. Sahenk Z, et al. AAV1.NT-3 gene therapy for charcot-marie-tooth neuropathy. *Mol Ther.* 2014;22(3):511-521.
 37. Sahenk Z, et al. Gene therapy to promote regeneration in Charcot-Marie-Tooth disease. *Brain Res.* 2020;1727:146533.
 38. Khajavi M, et al. Oral curcumin mitigates the clinical and neuropathologic phenotype of the Trembler-J mouse: a potential therapy for inherited neuropathy. *Am J Hum Genet.* 2007;81(3):438-453.
 39. Meyer zu Horste G, et al. Antiprogestone therapy uncouples axonal loss from demyelination in a transgenic rat model of CMT1A neuropathy. *Ann Neurol.* 2007;61(1):61-72.
 40. Verhamme C, et al. Oral high dose ascorbic acid treatment for one year in young CMT1A patients: a randomised, double-blind, placebo-controlled phase II trial. *BMC Med.* 2009;7:70.
 41. Madorsky I, et al. Intermittent fasting alleviates the neuropathic phenotype in a mouse model of Charcot-Marie-Tooth disease. *Neurobiol Dis.* 2009;34(1):146-154.
 42. Nobbio L, et al. P2X7-mediated increased intracellular calcium causes functional derangement in Schwann cells from rats with CMT1A neuropathy. *J Biol Chem.* 2009;284(34):23146-23158.
 43. Rangaraju S, et al. Rapamycin activates autophagy and improves myelination in explant cultures from neuropathic mice. *J Neurosci.* 2010;30(34):11388-11397.
 44. Chahbouni M, et al. Melatonin treatment normalizes plasma pro-inflammatory cytokines and nitrosative/oxidative stress in patients suffering from Duchenne muscular dystrophy. *J Pineal Res.* 2010;48(3):282-289.
 45. Pareyson D, et al. Ascorbic acid in Charcot-Marie-Tooth disease type 1A (CMT-TRIAAL and CMT-TRAUK): a double-blind randomised trial. *Lancet Neurol.* 2011;10(4):320-328.
 46. Kullenberg D, et al. Health effects of dietary phospholipids. *Lipids Health Dis.* 2012;11:3.
 47. Attarian S, et al. An exploratory randomised double-blind and placebo-controlled phase 2 study of a combination of baclofen, naltrexone and sorbitol (PXT3003) in patients with Charcot-Marie-Tooth disease type 1A. *Orphanet J Rare Dis.* 2014;9:199.
 48. Chumakov I, et al. Polytherapy with a combination of three repurposed drugs (PXT3003) down-regulates Pmp22 over-expression and improves myelination, axonal and functional parameters in models of CMT1A neuropathy. *Orphanet J Rare Dis.* 2014;9:201.
 49. Nicks J, et al. Rapamycin improves peripheral nerve myelination while it fails to benefit neuromuscular performance in neuropathic mice. *Neurobiol Dis.* 2014;70:224-236.
 50. Hantke J, et al. c-Jun activation in Schwann cells protects against loss of sensory axons in inherited neuropathy. *Brain.* 2014;137(pt 11):2922-2937.
 51. Ndong Ntoutoume GMA, et al. Development of curcumin-cyclodextrin/cellulose nanocrystals complexes: new anticancer drug delivery systems. *Bioorg Med Chem Lett.* 2016;26(3):941-945.
 52. Kieppura AJ, et al. Charcot-Marie-Tooth type 1A drug therapies: role of adenylyl cyclase activity and G-protein coupled receptors in disease pathomechanism. *Acta Neurobiol Exp (Wars).* 2018;78(3):198-209.
 53. Fledrich R, et al. Targeting myelin lipid metabolism as a potential therapeutic strategy in a model of CMT1A neuropathy. *Nat Commun.* 2018;9(1):3025.
 54. Prukop T, et al. Early short-term PXT3003 combinational therapy delays disease onset in a transgenic rat model of Charcot-Marie-Tooth disease 1A (CMT1A). *PLoS One.* 2019;14(1):e0209752.
 55. Fledrich R, et al. NRG1 type I dependent autocrine stimulation of Schwann cells in onion bulbs of peripheral neuropathies. *Nat Commun.* 2019;10(1):1467.
 56. Prukop T, et al. Synergistic PXT3003 therapy uncouples neuromuscular function from dysmyelination in male Charcot-Marie-Tooth disease type 1A (CMT1A) rats. *J Neurosci Res.* 2020;98(10):1933-1952.
 57. Ha N, et al. A novel histone deacetylase 6 inhibitor improves myelination of Schwann cells in a model of Charcot-Marie-Tooth disease type 1A. *Br J Pharmacol.* 2020;177(22):5096-5113.
 58. Caillaud M, et al. Curcumin-cyclodextrin/cellulose nanocrystals improve the phenotype of Charcot-Marie-Tooth-1A transgenic rats through the reduction of oxidative stress. *Free Radic Biol Med.* 2020;161:246-262.
 59. Park NY, et al. Farnesol ameliorates demyelinating phenotype in a cellular and animal model of Charcot-Marie-Tooth disease type 1A. *Curr Issues Mol Biol.* 2021;43(3):2011-2021.
 60. Attarian S, et al. A double-blind, placebo-controlled, randomized trial of PXT3003 for the treatment of Charcot-Marie-Tooth type 1A. *Orphanet J Rare Dis.* 2021;16(1):433.
 61. Stavrou M, et al. Emerging therapies for Charcot-Marie-Tooth inherited neuropathies. *Int J Mol Sci.* 2021;22(11):6048.
 62. Martinez NJ, et al. Genome-edited coincidence and PMP22-HiBiT fusion reporter cell lines enable an artifact-suppressive quantitative high-throughput screening strategy for PMP22 gene-dosage disorder drug discovery. *ACS Pharmacol Transl Sci.* 2021;4(4):1422-1436.
 63. Lee JS, et al. Targeted PMP22 TATA-box editing by CRISPR/Cas9 reduces demyelinating neuropathy of Charcot-Marie-Tooth disease type 1A in mice. *Nucleic Acids Res.* 2020;48(1):130-140.
 64. Hai M, et al. Competitive binding of triplex-forming oligonucleotides in the two alternate promoters of the PMP22 gene. *Antisense Nucleic Acid Drug Dev.* 2001;11(4):233-246.
 65. Lee JS, et al. Pmp22 mutant allele-specific siRNA alleviates demyelinating neuropathic phenotype in vivo. *Neurobiol Dis.* 2017;100:99-107.
 66. Zhao HT, et al. PMP22 antisense oligonucleotides reverse Charcot-Marie-Tooth disease type 1A features in rodent models. *J Clin Invest.* 2018;128(1):359-368.
 67. Boutary S, et al. Squalenoyl siRNA PMP22 nanoparticles are effective in treating mouse

- models of Charcot-Marie-Tooth disease type 1A. *Commun Biol.* 2021;4(1):317.
68. Boutary S, et al. Treating PMP22 gene duplication-related Charcot-Marie-Tooth disease: the past, the present and the future. *Transl Res.* 2021;227:100–111.
 69. Carrington JC, et al. Role of microRNAs in plant and animal development. *Science.* 2003;301(5631):336–338.
 70. He L, et al. MicroRNAs: small RNAs with a big role in gene regulation. *Nat Rev Genet.* 2004;5(7):522–531.
 71. Serfecz J, et al. Downregulation of the human peripheral myelin protein 22 gene by miR-29a in cellular models of Charcot-Marie-Tooth disease. *Gene Ther.* 2019;26(12):455–464.
 72. Lee JS, et al. miR-381 attenuates peripheral neuropathic phenotype caused by overexpression of PMP22. *Exp Neurobiol.* 2019;28(2):279–288.
 73. Gautier B, et al. AAV2/9-mediated silencing of PMP22 prevents the development of pathological features in a rat model of Charcot-Marie-Tooth disease 1A. *Nat Commun.* 2021;12(1):2356.
 74. Boudreau RL, et al. Rapid cloning and validation of microRNA shuttle vectors: a practical guide. In: Harper SQ, ed. *RNA Interference Technique.* Humana Springer Press; 2011:19–37.
 75. Wallace LM, et al. Pre-clinical safety and off-target studies to support translation of AAV-mediated RNAi therapy for FSHD. *Mol Ther Methods Clin Dev.* 2018;8:121–130.
 76. Schiza N, et al. Gene replacement therapy in a model of Charcot-Marie-Tooth 4C neuropathy. *Brain.* 2019;142(5):1227–1241.
 77. Kagiava A, et al. Gene replacement therapy after neuropathy onset provides therapeutic benefit in a model of CMT1X. *Hum Mol Genet.* 2019;28(21):3528–3542.
 78. Kagiava A, et al. AAV9-mediated Schwann cell-targeted gene therapy rescues a model of demyelinating neuropathy. *Gene Ther.* 2021;28(10–11):659–675.
 79. Rossor AM, et al. A longitudinal and cross-sectional study of plasma neurofilament light chain concentration in Charcot-Marie-Tooth disease. *J Peripher Nerv Syst.* 2021;27(1):50–57.
 80. Jeon H, et al. Cytokines secreted by mesenchymal stem cells reduce demyelination in an animal model of Charcot-Marie-Tooth disease. *Biochem Biophys Res Commun.* 2022;597:1–7.
 81. Jennings MJ, et al. NCAM1 and GDF15 are biomarkers of Charcot-Marie-Tooth disease in patients and mice [published online February 10, 2022]. *Brain.* <https://doi.org/10.1093/brain/awac055>.
 82. Kao ML, et al. Pharmacokinetics and distribution of 2-hydroxypropyl- β -cyclodextrin following a single intrathecal dose to cats. *J Inherit Metab Dis.* 2020;43(3):618–634.
 83. Bradbury AM, et al. Krabbe disease successfully treated via monotherapy of intrathecal gene therapy. *J Clin Invest.* 2020;130(9):4906–4920.
 84. Kagiava A, et al. Efficacy of AAV serotypes to target Schwann cells after intrathecal and intravenous delivery. *Sci Rep.* 2021;11(1):23358.
 85. Berciano J, et al. Clinico-electrophysiological correlation of extensor digitorum brevis muscle atrophy in children with charcot-marie-tooth disease 1A duplication. *Neuromuscul Disord.* 2000;10(6):419–424.
 86. Burns J, et al. Evolution of foot and ankle manifestations in children with CMT1A. *Muscle Nerve.* 2009;39(2):158–166.
 87. Verhamme C, et al. Clinical disease severity and axonal dysfunction in hereditary motor and sensory neuropathy Ia. *J Neurol.* 2004;251(12):1491–1497.
 88. Manganeli F, et al. Nerve conduction velocity in CMT1A: what else can we tell? *Eur J Neurol.* 2016;23(10):1566–1571.
 89. Perea J, et al. Induced myelination and demyelination in a conditional mouse model of Charcot-Marie-Tooth disease type 1A. *Hum Mol Genet.* 2001;10(10):1007–1018.
 90. Maier M, et al. Distinct elements of the peripheral myelin protein 22 (PMP22) promoter regulate expression in Schwann cells and sensory neurons. *Mol Cell Neurosci.* 2003;24(3):803–817.
 91. Roux KJ, et al. The temporospatial expression of peripheral myelin protein 22 at the developing blood-nerve and blood-brain barriers. *J Comp Neurol.* 2004;474(4):578–588.
 92. Stavrou M, et al. Genetic mechanisms of peripheral nerve disease. *Neurosci Lett.* 2021;742:135357.
 93. Naveed A, et al. Onasemnogene abeparvovec (AVXS-101) for the treatment of spinal muscular atrophy. *J Pediatr Pharmacol Ther.* 2021;26(5):437–444.
 94. Bailey RM, et al. Development of intrathecal AAV9 gene therapy for giant axonal neuropathy. *Mol Ther Methods Clin Dev.* 2018;9:160–171.
 95. Sancho S, et al. Distal axonopathy in peripheral nerves of PMP22-mutant mice. *Brain.* 1999;122(pt 8):1563–1577.
 96. Jeng CL, et al. Intraneural injections and regional anesthesia: the known and the unknown. *Minerva Anesthesiol.* 2011;77(1):54–58.
 97. Meyer K, et al. Improving single injection CSF delivery of AAV9-mediated gene therapy for SMA: a dose-response study in mice and nonhuman primates. *Mol Ther.* 2015;23(3):477–487.
 98. Mendell JR, et al. Single-dose gene-replacement therapy for spinal muscular atrophy. *N Engl J Med.* 2017;377(18):1713–1722.
 99. Al-Zaidy SA, et al. From clinical trials to clinical practice: practical considerations for gene replacement therapy in SMA type 1. *Pediatr Neurol.* 2019;100:3–11.
 100. Van Alstynne M, et al. Gain of toxic function by long-term AAV9-mediated SMN overexpression in the sensorimotor circuit. *Nat Neurosci.* 2021;24(7):930–940.
 101. Keiser MS, et al. Toxicity after AAV delivery of RNAi expression constructs into nonhuman primate brain. *Nat Med.* 2021;27(11):1982–1989.
 102. Hordeaux J, et al. Adeno-associated virus-induced dorsal root ganglion pathology. *Hum Gene Ther.* 2020;31(15–16):808–818.
 103. de Visser M, et al. Ascorbic acid for treatment in CMT1A: what's next? *Lancet Neurol.* 2011;10(4):291–293.
 104. Bren L. The importance of patient-reported outcomes...it's all about the patients. *FDA Consum.* 2006;40(6):26–32.
 105. Menotti F, et al. Amount and intensity of daily living activities in Charcot-Marie-Tooth 1A patients. *Brain Behav.* 2014;4(1):14–20.
 106. Padua L, et al. Novel outcome measures for Charcot-Marie-Tooth disease: validation and reliability of the 6-min walk test and Step-WatchTM Activity Monitor and identification of the walking features related to higher quality of life. *Eur J Neurol.* 2016;23(8):1343–1350.
 107. Johnson NE, et al. The Charcot-Marie-Tooth health index: evaluation of a patient-reported outcome. *Ann Neurol.* 2018;84(2):225–233.
 108. Morrow JM, et al. Validation of MRC Centre MRI calf muscle fat fraction protocol as an outcome measure in CMT1A. *Neurology.* 2018;91(12):e1125–e1129.
 109. Sandelius A, et al. Plasma neurofilament light chain concentration in the inherited peripheral neuropathies. *Neurology.* 2018;90(6):e518–e524.
 110. Millere E, et al. Plasma neurofilament light chain as a potential biomarker in Charcot-Marie-Tooth disease. *Eur J Neurol.* 2021;28(3):974–981.
 111. Fledrich R, et al. Biomarkers predict outcome in Charcot-Marie-Tooth disease 1A. *J Neurol Neurosurg Psychiatry.* 2017;88(11):941–952.
 112. Wang D, et al. Adeno-associated virus vector as a platform for gene therapy delivery. *Nat Rev Drug Discov.* 2019;18(5):358–378.
 113. Visigalli D, et al. Exploiting Sphingo- and glycerophospholipid impairment to select effective drugs and biomarkers for CMT1A. *Front Neurol.* 2020;11:903.